Modelling of Methane-Rich Gas Pipeline Networks for Simulation and Control

A.J. Wiid[a], J.D. le Roux[a], I.K. Craig[a,*]

[a]*Department of Electrical, Electronic, and Computer Engineering, University of Pretoria, Pretoria, South Africa.*

Abstract

A non-linear model is developed to capture the transient flow and pressure behaviour of methane-rich gas (MRG) in industrial pipelines for the use in simulation and control applications. Hyperbolic partial differential equations describe the pipe pressure and flow profiles, and composition analyses are used to develop the physical properties of the gas appearing in the pipe segment equations. The spectral element method (SEM) is used to numerically solve the spatial profiles within the pipeline, and a model verification is done on the SEM tuning parameter choices. The model is developed into a compact state-space description for improved usability. Furthermore, the developed model achieves good accuracy when validated on real process data of an industrial MRG network and can be used for simulation and model-based control applications.

Keywords: control applications; methane-rich gas; modelling; natural gas; non-linear; pipeline networks; process control; spectral element method

1. Introduction

Industrial pipelines are used to transfer gas between suppliers and consumers. This may consist of a single pipe connecting two nodes or a network of pipes and nodes.

Gas pipelines are traditionally controlled by regulatory control loops which experience various control challenges such as varying disturbance sizes due to upsets and changing operating regions. Regulatory control loops generally have difficulty in meeting pressure set-point control and flow stability objectives simultaneously over large operating regions. Additionally, these pipe-line networks are multivariate with multiple interactive suppliers and consumers with different control priorities depending on their associated economic value.

Methane-rich gas (MRG) and natural gas (NG) are both used as a feedstock to the pipeline network in this study. They are similar in composition but originate from different sources. MRG is a product of upstream cryogenic distillation units and the Fischer–Tropsch reaction which receives gasified coal as a feedstock [2]. NG is a fossil fuel extracted from underground reservoirs and is the secondary feedstock in the network. MRG is used as the primary feedstock in autothermal reforming and as a utility for make-up in fuel gas blending to maintain a specified Wobbe index [3], [4]. MRG is also sold as an end product to external consumers.

Due to pressure set-point control, the regulatory control scheme uses flaring for over-pressure control during fast disturbances to protect the downstream units from flow upsets.

This wastes valuable feedstock and causes expensive economic penalties. It is therefore advisable to utilise the buffering capabilities of the header inventory by manipulating all available controlled flows in a co-ordinated manner to meet control and economic objectives.

Model predictive control (MPC) is an attractive and widely accepted solution which may address these challenges [4]. However, a suitable MPC requires a dynamic model which is accurate over large operating regions, can accurately predict fast transients, and can appropriately compensate for changes in gas composition. The development of such a model is the main focus of this study.

The gas composition is usually assumed to be constant in literature [5], [6], [7]. This in turn implicitly assumes constant standard values for the composition dependant gas properties. In contrast, this study has access to online analysers on the feed streams which provide composition measurements and are used to calculate the gas properties as inputs to the model.

The pressure and flow profiles within the pipelines can vary considerably due to the compressible nature of gasses. Such conditions are difficult to model truthfully over large non-linear regions and require accurate numerically convergent schemes to solve the relevant partial differential equations. In order to accurately represent the spatial profile, short spatial steps are needed and in turn, due to the strict Courant-Friedrichs-Lewy (CFL) condition [8], it is important to discretise the temporal steps appropriately which can be computationally expensive.

There are numerous numerical methods for solving partial differential equations, such as finite difference [9], finite volume [10], spectral [11], and finite element methods (FEM) [12]. The spectral element method (SEM) [13] is particularly attractive for spatial discretisation because of the following: the solution algorithms are inherently stable, high numerical accuracy can be achieved, relatively few elements are required, and it is valid

---

over a broad range of conditions. It achieves this by combining the adaptivity of the finite element method and the accuracy and high convergence rate of spectral methods. In practice, it is important for models used in the simulation and control of gas pipeline networks to be computationally efficient [14], [15], [16], [17]. To aid this consideration, methods employed to increase the computational efficiency of the proposed model will be highlighted during the model development.

The modelling of NG pipelines has been approached in various ways. [15] uses radial basis function surrogates and proper orthogonal decomposition reduction techniques to reduce the computational cost and complexity of the network models. A rough discretisation method is employed together with steady-state mass balances around the pressure nodes. The methods used are compared to the isothermal governing equations. [16] uses electronic circuit concepts of resistance, capacitance, and inductance to reduce the governing equations into first order ordinary differential equations which reduces the computational effort and model complexity. [18] developed a linear state-space description using a lumped-parameter model and Taylor approximations in order to reduce the computational effort and complexity while retaining sufficient accuracy for large networks. [5], [19] uses third-degree Hermite polynomials to spatially discretise the pipelines and use complementaries to model the non-smooth absolute flow and friction terms in the momentum balance. [20] linearises the governing equations and implements the Laplace transform to solve the temporal problem. The pipeline is then spatially discretised and solved using explicit finite difference methods. [6] uses the non-isothermal governing equations which includes the energy balance and uses the orthogonal collocation method to solve the partial differential equations. [21] accounts for pipe inclinations in the governing equations and uses the method of characteristics and the Crank-Nicolson method to solve the partial differential equations in a Matlab-Simulink simulation environment. [7] uses a totally implicit method to discretise the governing equations and particle-swarm optimisation to calculate solutions for flow rates. [22] uses a least squares spectral method to model NG pipeline transients. [23], [24] use a high order FEM and an implicit time discretisation scheme on large NG pipelines. [25] uses traditional volume-based approaches to solve the governing equations and developed an energy formulation based on the gas heating value which also allows for variable gas composition in pipes which result from gas mixing. [26] uses implicit finite difference methods to solve the non-isothermal governing equations and accounts for variable composition due to hydrogen injection. [27] uses a finite difference scheme to discretise the pipeline and an implicit Euler method for the temporal solution which is also used in [28]. The model is then used to dynamically optimise a gas network under composition and demand uncertainty. [29] uses a pseudo-spectral discretisation of the governing equations and reduces the model using lumped elements. The model is used for optimal control. [17] provides a thorough study of different gas pipeline models, the impact of simplifying assumptions, and specifically compares isothermal and non-isothermal models.

The work developed in this study is a continuation of [1] in

which the development of a non-linear model for MRG networks is described and validated on an industrial MRG network. A trapezoidal spatial approximation was used for the pipelines and dynamic mass balances around the nodes were used to model the pressures. This model can be numerically sensitive to fast dynamics due to the CFL condition not being accounted for. As an improvement the SEM proposed by [8] for hydraulic simulations is applied to the MRG network in [1] and explicitly discretised in time. This improvement implicitly incorporates the CFL condition and allows for bi-directional flow due to the inclusion of the absolute term in the momentum equation which is not possible in [1]. In contrast, [1] uses an equivalent length [30] as a fitting parameter by fitting a steady-state pressure drop equation to plant data with a least squares minimisation algorithm [31]. This results in exaggerated pipe lengths to compensate for the pressure drop due to pipe components which influences the pipe volume and therefore induces additional lag into the dynamic flow profiles. This is reasonable in [1] due to the simplification of the momentum equation where the flow differentials are neglected. However, the momentum equation is not similarly simplified in the current work. As an improvement a resistance coefficient [32] is used as an additional fitting parameter. The parameters are estimated in the current work by minimising the output error prediction with a single shooting technique [33], [34].

The contribution of this paper is the presentation of an accurate and numerically robust model which can be applied to MRG and NG pipelines, and is validated on an industrial MRG network. The development of reasonable models which are complex enough to accurately represent real systems but are simple enough to be practically applied is difficult. This study aims to capture many of the physical parameter variations observed in real world systems and presents the final model as a practically implementable solution. To this end the model is developed into an explicit state-space representation which is ideal for simulation and control applications. Assumptions made in the modelling process are stated so that the model can be adapted to individual applications.

The paper is organised as follows: Section 2 introduces the governing equations, defines the gas properties required for the component model derivations, and describes the various components models. The SEM is used in Section 3 to spatially solve the governing equations given in Section 2. A state-space description of the overall system of equations is derived in Section 4 from the equations given in Section 3. In addition, discretised temporal variables are used to develop a time propagation algorithm, and a model verification is done on the SEM. Section 5 describes the model validation, and the parameter estimation on an industrial MRG network using real data as inputs. Section 6 concludes the paper and outlines future work.

2. Pipeline Model Development

In this section the governing equations, gas properties and model components are described which are used in subsequent sections. The nomenclature that is used in the model development is given in Table 1.

Table 1: Nomenclature.

Symbol	Description	Units	Symbol	Description	Units
P	Pressure	Pa	v_p	Linear velocity	m/s
Q	Flow	kg/s	μ	Viscosity	cP
Z	Compressibility	-	ρ	Density	kg/m^3
R	Gas constant	J/kmolK	Re	Reynolds number	-
T	Temperature	K	f	Friction factor	-
K_G	Resistance coeff.	m^{-1}	y	Molar fraction	-
A	Cross section area	m^2	V	Volume	m^3
M_w	Molecular weight	kg/kmol	L	Pipe length	m
D	Diameter	m	ε	Pipe roughness	mm
W_c	Compressor power	W	C_p	Specific heat capacity	J/kgK
γ	Specific heats ratio	-	n_c	Compressor efficiency	-
m	Gas mass	kg	Q_c	Compressor flow	kg/s

2.1. Governing Equations

The temporal (t) and spatial (z) profiles of pressure P and flow Q within a well-insulated pipe segment are described by,

$$\frac{\partial P}{\partial t} + \frac{ZRT}{AM_w}\frac{\partial Q}{\partial z} = 0, \tag{1a}$$

$$\frac{\partial Q}{\partial t} + A\frac{\partial P}{\partial z} + \frac{fZRTQ|Q|}{2DAM_wP} = 0, \tag{1b}$$

$$PAL - \frac{mZRT}{M_w} = 0, \tag{1c}$$

where (1a) and (1b) represent the continuity and momentum equations respectively [5], [20]. The gas properties are related to each other within the pipe with an equation of state (1c), in particular, the ideal gas law compensated for compressibility is used. Parameter R is the gas constant, A is the cross sectional area of the pipe, Z is the gas compressibility, T is the temperature, f is the coefficient of friction, D the pipe diameter, M_w is the mixed gas molecular weight, m the gas mass, and L the pipe length. For ease of presentation, the spatial and temporal dependencies of the variables are suppressed in the text.

This formulation of the governing equations was simplified by excluding the contribution of convective inertia to the spatial pressure losses in (1b) because the contribution of convective inertia is negligible compared to the pipe frictional losses [16], [20]. The contribution of the gas inertia term $\frac{\partial Q}{\partial t}$ can also be excluded [5] but was included in this work to capture the transient flow behaviour. Additionally, the energy governing equation is excluded because the pipes are assumed to be well insulated such that temperature losses are negligible.

2.2. Gas Properties

The composition analysis of the MRG and NG streams are used to calculate the gas properties needed in future calculations. The mole fraction weighted average molar mass of the mixed gas is defined as,

$$M_w = \sum_i^N M_i y_i, \tag{2}$$

where y_i is the molar fraction and M_i the molar mass of the ith gas component. The pseudo-critical temperatures T_{pc}, pressures P_{pc} and volumes V_{pc} are similarly calculated as [35], [36],

$$T_{pc} = \sum_i^N y_i T_{ci}, \quad P_{pc} = \sum_i^N y_i P_{ci}, \quad V_{pc} = \sum_i^N y_i V_{ci}, \tag{3}$$

where T_{ci}, P_{ci}, and V_{ci} is the critical temperature, pressure, and volume of gas component i respectively. The pseudo-reduced temperatures T_{pr}, pressures P_{pr}, and volumes V_{pr} are calculated as,

$$T_{pr} = \frac{T}{T_{pc}}, \quad P_{pr} = \frac{P}{P_{pc}}, \quad V_{pr} = \frac{V}{V_{pc}}. \tag{4}$$

The pseudo-critical gas density ρ_{pc} and pseudo-reduced gas density ρ_{pr} can be calculated as,

$$\rho_{pc} = \frac{M_w}{V_{pc}}, \quad \rho_{pr} = \frac{\rho}{\rho_{pc}}. \tag{5}$$

The pseudo-critical properties of the pure components are dimensionless constants which can be found in literature [37]. The gas density ρ can be derived from (1c) as,

$$\rho = \frac{m}{AL} = \frac{M_w P}{ZRT}. \tag{6}$$

2.3. Gas Compressibility

To avoid an iterative approach to estimating the gas properties, an empirical equation is used to calculate Z as opposed to an equation of state. The pseudo reduced temperature and pressure of the mixed gas are given as inputs to infer the compressibility explicitly from an equation correlated with experimental data. The equation is valid for $P_{pr} \in [0.2 : 15]$ and $T_{pr} \in [1.05 : 3]$ [35],

$$Z = \frac{D_Z P_{pr}(1 + y_Z + y_Z^2 - y_Z^3)}{(D_Z P_{pr} + E_Z y_Z^2 - F_Z y_Z^{G_Z})(1 - y_Z)^3}, \tag{7a}$$

$$y_Z = \frac{D_Z P_{pr}}{\frac{1+A_Z^2}{C_Z} - \frac{A_Z^2 B_Z}{C_Z^3}}. \tag{7b}$$

The terms A_Z, B_Z, C_Z, D_Z, E_Z, F_Z, and G_Z are tuning constants used to fit experimental data. The terms denoted by Z to indicate the relation to compressibility terms are given in [35]. Equation (7) was chosen because it correlates well with experimental data, is applicable over large ranges, can be explicitly implemented, and it is continuous.

2.4. Viscosity

The equation for gas viscosity μ is based on the kinetic theory of gasses (see e.g. [36]), and is given by,

$$\mu = B_\mu \sqrt{M_{sqrt}} \sqrt{T_{pr}} \exp\left(\frac{\theta + (A_b + A_k T_{pr})\rho_r^\alpha}{T_{pr}}\right), \tag{8}$$

where,

$$\sqrt{M_{sqrt}} = \sum_{i}^{N} \sqrt{M_i}\, y_i. \qquad (9)$$

The parameters B_μ, θ, A_b, A_k, and α are tuning parameters used to fit the first principles model to experimental data and is fully described in [36].

2.5. Coefficient of Friction

The Darcy-Weisbach friction factor f_D is given in [38],

$$f_D = 8\left(\left(\frac{8}{Re}\right)^{12} + \frac{1}{(A_f + B_f)^{1.5}}\right)^{\frac{1}{12}}, \qquad (10a)$$

$$A_f = \left(-2.457\ln\left(\frac{7}{Re}\right)^{0.9} + 0.27\left(\frac{\varepsilon}{D}\right)\right)^{16}, \qquad (10b)$$

$$B_f = \left(\frac{37530}{Re}\right)^{16}, \qquad (10c)$$

where Re is the Reynolds number. The pipe roughness ε is chosen to be 0.0457 mm [39]. The advantage of using (10) is that it is an explicit formula and holds for both the laminar and turbulent flow regimes, and gives unique and reasonable results in the transitional regime [39]. This eliminates the need to confirm the flow regime and then choose an appropriate friction factor. Additionally, the need to use complementaries to smooth out the calculation between flow regimes is eliminated. The Reynolds number is calculated as,

$$Re = \frac{\rho v_p L}{\mu}. \qquad (11)$$

2.6. Equivalent Length and Resistance Coefficient

The pipe architecture components (e.g. bends, T-pieces, and reducers), and utility components (e.g. block valves, measurement orifices, and check-valves) should be considered in the modelling as these components have an impact on the total frictional resistance in the pipe. There are generally two methods to compensate for the additional resistance due to the pipe components: the equivalent length method and the equivalent resistance coefficient method [32]. The equivalent length method calculates the length of a pipe section which will render the same pressure loss as a given restriction. The equivalent resistance coefficient method determines the additional frictional resistance that a given component generates. Equivalent pipe lengths and resistance coefficients are determined experimentally for various pipe components and given literature [30], [32].

The pipe lengths used in the model are calculated as the global equivalent pipe length L_G added to the real pipe length L_r,

$$L = L_r + L_G. \qquad (12)$$

The friction factor used in the model is the sum of the Darcy-Weisbach friction factor f_D calculated in (10), and the resistance due to pipe components f_G,

$$f = f_D + f_G. \qquad (13)$$

The subscript G refers to the global contribution of all the individual components. f_G is dependent on flow and is calculated as,

$$f_G = K_G \frac{D}{L} \frac{v_p^2}{2g}, \qquad (14)$$

where K_G is the resistance coefficient due to the pipe components, and g is the gravitational acceleration. L_G and K_G can be calculated if the pipe components are known but are used as fitting parameters to fit the model to data as done in this study.

2.7. Compressors

Compressor power consumption is calculated as [5],

$$W_c = \frac{Q_c C_p T_i}{n_c}\left(\left(\frac{P_o}{P_i}\right)^{\frac{\gamma-1}{\gamma}} - 1\right), \qquad (15)$$

where W_c is the power consumption, C_p is the specific heat capacity of the gas, Q_c is the mass flow rate through the compressor, T_i is the inlet temperature, n_c is the compressor efficiency, P_o is the discharge pressure, P_i is the suction pressure, and γ is the ratio of specific heats. The flow direction is fixed and it is assumed that the compressor has negligible volume.

3. Spatial Solution: Spectral Element Method

The analytic equations in Section 2 will now be solved spatially by means of the SEM. This is done in Section 3.1 by obtaining the weak formulation of (1a) and (1b) as per the Galerkin Method. The weak formulation is discretised spatially in Section 3.2, and mapped to an appropriate co-ordinate system in Section 3.3. Lagrange polynomials are used as basis functions in Section 3.4 to approximate the analytical functions in Section 3.1. The integrals of the discretised pipe segments in Section 3.2 are approximated in Section 3.5 using the quadrature rule. The mass and stiffness matrices are assembled in Section 3.6 followed by a description of the global system of equations in Section 3.7, and boundary conditions in Section 3.8.

3.1. Weak Formulation of Governing Equations

The pipe segment equations (1a) and (1b) can be written in conservative form as,

$$\frac{\partial}{\partial t}\begin{bmatrix}\kappa P \\ \sigma Q\end{bmatrix} + \frac{\partial}{\partial z}\begin{bmatrix}0 & 1/\sigma \\ 1/\kappa & 0\end{bmatrix}\begin{bmatrix}\kappa P \\ \sigma Q\end{bmatrix} = -\begin{bmatrix}0 \\ \tau\,\Theta\end{bmatrix}, \qquad (16)$$

where,

$$\kappa = \frac{AM_w}{ZRT}, \quad \sigma = \frac{1}{A}, \quad \tau = \frac{\sigma f ZRT}{2DAM_w}, \quad \Theta = \frac{Q|Q|}{P}. \qquad (17)$$

To obtain the weak formulation, the Galerkin projection methodology is followed where (16) is integrated and multiplied by a suitable set of test functions υ on the interval $[0, L]$. The weak formulation is,

$$\int_0^L \left[\frac{\partial}{\partial t}\begin{bmatrix}\kappa P \\ \sigma Q\end{bmatrix} + \frac{\partial}{\partial z}\begin{bmatrix}0 & 1/\sigma \\ 1/\kappa & 0\end{bmatrix}\begin{bmatrix}\kappa P \\ \sigma Q\end{bmatrix} + \begin{bmatrix}0 \\ \tau\,\Theta\end{bmatrix}\right]\upsilon\, dz = 0. \qquad (18)$$

4

Applying integration by parts, (18) can be expressed as,

$$\int_0^L \frac{\partial}{\partial t}\begin{bmatrix} \kappa P \\ \sigma Q \end{bmatrix} \upsilon dz = \int_0^L \begin{bmatrix} Q \\ P \end{bmatrix}\frac{\partial \upsilon}{\partial z} dz$$
$$- \int_0^L \begin{bmatrix} 0 \\ \tau \Theta \end{bmatrix} \upsilon dz - \begin{bmatrix} Q \\ P \end{bmatrix}\Big|_0^L \upsilon. \qquad (19)$$

3.2. Spatial Discretisation into Elements

The weak formulation in (19) is partitioned into n elements denoted by Ω^e such that $\Omega^e = [z_{n-1}, z_n]$, with $0 = z_0 < z_1 < \cdots < z_n = L$. This results in,

$$\int_{\Omega^e} \frac{\partial}{\partial t}\begin{bmatrix} \kappa P \\ \sigma Q \end{bmatrix} \upsilon dz = \int_{\Omega^e} \begin{bmatrix} Q \\ P \end{bmatrix}\frac{\partial \upsilon}{\partial z} dz - \int_{\Omega^e} \begin{bmatrix} 0 \\ \tau \Theta \end{bmatrix} \upsilon dz, \qquad (20)$$

for $e = \{1, \dots, n\}$. The number of elements chosen is a tuning factor known as h-refinement. For a homogeneous medium the elements are chosen to be the same length. It is computationally advantageous to vary the element segment lengths along a heterogeneous medium by adapting the spatial mesh to the wave velocities, thereby achieving the same accuracy for less computational effort [40]. If the pipes are sufficiently long and the properties change substantially along the pipe due to compressibility, it can be exploited by increasing the element length as the linear velocity decreases. Mathematically this is done by defining [12],

$$\Delta z_k = \alpha^{(k-1)}\Delta z_1, \quad \text{for} \quad k = 1, \dots, n, \qquad (21)$$

where,

$$\alpha = r^{1/(n-1)}, \quad \text{and} \quad r \equiv \frac{\Delta z_n}{\Delta z_1}. \qquad (22)$$

The first element size is calculated explicitly as,

$$\Delta z_1 = \frac{1 - \alpha}{1 - \alpha^n}L. \qquad (23)$$

By choosing the tuning factor r as the ratio between the first and last element lengths, the desired spatial mesh is generated over the pipe length.

3.3. Mapping of Element Functions

By making use of the mapping function described as,

$$F(\xi)_e = \frac{z_n - z_{n-1}}{2}\xi + \frac{z_n - z_{n-1}}{2}, \qquad (24)$$

where the element global co-ordinates, z_n and z_{n-1} for each element, are mapped to a local co-ordinate system $\xi \in \Lambda$ in the interval $\Lambda = [-1, 1]$. To account for the co-ordinate transformation inside the integral in (20), the functions have to be multiplied by the Jacobian which, for the one-dimensional case and varying element lengths, can be defined as,

$$J^e = \frac{dz}{d\xi} = \frac{z_n - z_{n-1}}{2}. \qquad (25)$$

The co-ordinate transforms of the spatial dependant element functions, $f(z) \in \{P, Q, \frac{\partial P}{\partial t}, \frac{\partial Q}{\partial t}, \Theta, \text{and } \upsilon\}$, are e.g. integrated as,

$$\int_{\Omega^e} f^e(z)dz = \int_{\Lambda} f^e(\xi)\frac{dz}{d\xi}d\xi = \int_{-1}^1 f^e(\xi)J^e d\xi. \qquad (26)$$

The points ξ are chosen as the collocation points of the Gauss-Lobatto-Legendre (GLL) quadrature [12].

3.4. Interpolation of Element Functions

To approximate the analytical functions in (19), Lagrange polynomials are used as interpolating functions which are, for a polynomial of order N, defined as,

$$\ell_i^N(\xi) = \prod_{j \neq i}^N \frac{\xi - \xi_j}{\xi_i - \xi_j}, \quad \text{for} \quad i, j = 0, \dots, N. \qquad (27)$$

In order to improve the performance of the numerical scheme, Barycentric Lagrange interpolation is used [41],

$$\ell_j^N(\xi) = \frac{w_j}{\xi - \xi_j} \Big/ \sum_{i=0}^N \frac{w_i}{\xi - \xi_i}, \qquad (28)$$

where the Barycentric weights w_j are defined by,

$$w_j = \frac{1}{\prod_{k \neq j} \xi_j - \xi_k}. \qquad (29)$$

It is important to note the following property of Lagrange polynomials,

$$\ell_i^N(\xi_j) = \delta_{i,j}, \quad \text{for } j = 0, \dots, N. \qquad (30)$$

where $\delta_{i,j}$ is the Kronecker Delta. Exploiting this property is one of the reasons why the SEM is computationally attractive. The superscript N remains the same and will be omitted for ease of presentation. The element functions $f^e(\xi)$ are approximated using the interpolation scheme as,

$$f^e(\xi) \approx \sum_{i=0}^N f^e(\xi_i)\ell_i(\xi), \qquad (31)$$

where f^e is restricted to the segment $[z_k, z_{k+1}]$. Similarly the spatial derivatives are approximated using,

$$\frac{df^e(\xi)}{dz} \approx \sum_{i=0}^N f^e(\xi_i)\ell_i'(\xi), \qquad (32)$$

where the first derivative of the Lagrange polynomial $\ell_i'(\xi)$ can be derived from the Barycentric Lagrange interpolation definition as,

$$\ell_i'(\xi_j) = \frac{w_i}{w_j}\frac{1}{\xi_j - \xi_i}, \quad \ell_i'(\xi_i) = -\sum_{i \neq j} \ell_i'(\xi_j). \qquad (33)$$

Computationally it is advantageous to compile the differentiation matrix $D^{(1)}$ once and reference the row-column location as needed. $D^{(1)}$ is defined as,

$$D_{ik}^{(1)} = \ell_i'(\xi_k). \qquad (34)$$

3.5. Integration of Functions over Elements

Integration over each element in the interval $[-1, 1]$ is performed by making use of the GLL quadrature of integration by approximating the integral as a weighted sum defined as,

$$\int_{\Lambda} f^e(\xi)d\xi \approx \sum_{k=0}^N \omega_k f(\xi_k), \qquad (35)$$

where ξ_k and ω_k are the collocation points and integration weights of the GLL quadrature of order N respectively. A Legendre polynomial of degree N is used to derive the collocation points,

$$P_N(\xi) = \frac{1}{2^N N!} \frac{d^N}{d\xi^N}(\xi^2 - 1)^N. \tag{36}$$

The collocation points used in the interpolation and integration can be calculated as the zeros of,

$$P'_N(\xi)(1 - \xi)^2, \tag{37}$$

where P'_N is the derivative of P_N. The integration weights, ω_k, are the weights of the GLL quadrature calculated as,

$$\omega_k = \begin{cases} 2[N^2 + N]^{-1}, & \xi_i = \pm 1, \\ 2[(N^2 + N)P_N^2(\xi_i)]^{-1}, & \xi_i \neq \pm 1. \end{cases} \tag{38}$$

The integration weights and collocation points are pre-calculated and tabulated to improve computational efficiency. Calculated values are also available in literature [12], [40]. Using the same collocation points for the interpolation and integration is one of the computational advantages of the SEM.

3.6. Matrix Assembly

The results from Sections 3.3, 3.4 and 3.5 can be applied to (20) to derive the elemental mass matrices as,

$$(M_\phi)_{ij}^e = \sum_{i=0}^N \sum_{k=0}^N \phi_i(\xi_k)\omega_k J(\xi_k)\delta_{i,j}, \quad \text{for } j = 0, \ldots, N. \tag{39}$$

where $\phi \in \{\kappa, \sigma, \tau\}$. The mass matrices are diagonal and non-singular. Therefore, the mass matrices can be inverted and stored as vectors to improve computational efficiency. Similar to the mass matrices, the elemental stiffness matrices can be derived as,

$$S_{ij}^e = \sum_{i=0}^N \sum_{k=0}^N \omega_k \ell'_i(\xi_k)\delta_{j,k}, \quad \text{for } j = 0, \ldots, N. \tag{40}$$

The global mass and stiffness matrices are assembled by diagonally combining n elemental matrices of size $[(N+1) \times (N+1)]$ into one $[(nN + 1) \times (nN + 1)]$ sized global matrix. This is illustrated using the assembly operator $\mathcal{A}$,

$$M_\phi = \mathop{\mathcal{A}}_{e=1}^n (M_\phi^e), \quad S = \mathop{\mathcal{A}}_{e=1}^n (S^e). \tag{41}$$

The elemental matrices overlap at the diagonal positions $i^{e+1}, j^{e+1} = 0$ and $i^e, j^e = N$ for $e \in \{1, \ldots, n-1\}$. The values at these locations are added.

3.7. Global System

The final global system of equations are,

$$M_\kappa \frac{d\boldsymbol{P}}{dt} = S\boldsymbol{Q} + Q_z \boldsymbol{b_0} - Q_L \boldsymbol{b_L}, \tag{42a}$$

$$M_\sigma \frac{d\boldsymbol{Q}}{dt} = S\boldsymbol{P} - M_\tau \boldsymbol{\Theta} + P_z \boldsymbol{b_0} - P_L \boldsymbol{b_L}. \tag{42b}$$

where the vectors indicated in bold are defined as,

$$\boldsymbol{P} = [P_1, \ldots, P_j]^T, \tag{43a}$$

$$\boldsymbol{Q} = [Q_1, \ldots, Q_j]^T, \tag{43b}$$

$$\boldsymbol{\Theta} = \left[\frac{Q_1|Q_1|}{P_1}, \ldots, \frac{Q_j|Q_j|}{P_j} \right]^T, \tag{43c}$$

and j is equal to the total number of collocation points. The boundary vectors are of the same length and are defined as,

$$\boldsymbol{b_0} = [1, 0, \ldots, 0]^T, \tag{44a}$$

$$\boldsymbol{b_L} = [0, \ldots, 0, 1]^T. \tag{44b}$$

The boundary conditions Q_z, Q_L, P_z, and P_L for a pipe segment of length L is defined as,

$$Q_z = Q(0, t) \quad \text{and} \quad Q_L = Q(L, t), \tag{45a}$$

$$P_z = P(0, t) \quad \text{and} \quad P_L = P(L, t). \tag{45b}$$

3.8. Boundary Conditions

Direchlet boundary conditions are used at the pipe end points. The authors of [8] recommend that the Lax-Friedrichs flux be used when solving (19) and give appropriate substitutions based on if the pressures or flows are chosen as boundary conditions. The following substitutions are made if the pipe inlet and outlet flows, $Q_{In}(t)$ and $Q_{Out}(t)$ respectively, are chosen as inputs,

$$Q_z = Q_{In}(t), \tag{46a}$$

$$P_z = P_1 - \sqrt{\frac{ZRT}{M_w}} \frac{AM_w}{2ZRT}(Q_1 - Q_{In}(t)), \tag{46b}$$

$$Q_L = Q_{Out}(t), \tag{46c}$$

$$P_L = P_j - \sqrt{\frac{ZRT}{M_w}} \frac{AM_w}{2ZRT}(Q_{Out}(t) - Q_j). \tag{46d}$$

It is important to note that either the pressure or flow must be specified at the boundary. The unspecified inputs are calculated using the numerical flux to improve numerical convergence as described by [8].

4. Temporal Solution

The equations in (42) are temporally discretised and developed into a state-space description.

4.1. State-Space Description

The temporal and spatial dependencies are shown in the input and output vector definitions for clarity. The model inputs are given by the input vector $\boldsymbol{u}$ as,

$$\boldsymbol{u} = [P_z(t), Q_z(t), P_L(t), Q_L(t), \boldsymbol{y}_z^T, T_z]^T. \tag{47}$$

The measured temperature at the pipe inlet T_z, and composition analysis $\boldsymbol{y}_z$ are used in the model calculations and governing equations at each sample interval. The measurements are

assumed to be constant with respect to pipe length and time between sample intervals. Note that y_z is a vector containing the molar fractions of the i pure components at the pipe inlet,

$$\boldsymbol{y}_z = [y_1, \ldots, y_i]^T.$$

The spatial flow and pressure vectors in (43) are grouped into the state vector,

$$\boldsymbol{x} = [\boldsymbol{P}(z,t)^T, \boldsymbol{Q}(z,t)^T]^T. \tag{48}$$

Additionally the model parameter vector $\boldsymbol{p}$ is defined as,

$$\boldsymbol{p} = [Z, f_D, M_w]^T, \tag{49}$$

and calculated from the inputs as described in Section 2. The state derivatives are written as,

$$\frac{d\boldsymbol{P}}{dt} = M_\kappa^{-1}[S\boldsymbol{Q} + Q_z\boldsymbol{b_0} - Q_L\boldsymbol{b_L}],$$
$$\frac{d\boldsymbol{Q}}{dt} = M_\sigma^{-1}[S\boldsymbol{P} - M_\tau\boldsymbol{\Theta} + P_z\boldsymbol{b_0} - P_L\boldsymbol{b_L}],$$

and in condensed form,

$$\dot{\boldsymbol{x}} = \boldsymbol{f}(\boldsymbol{x}, \boldsymbol{u}, \boldsymbol{p}). \tag{50}$$

The outputs are the pipe inlet and outlet pressures extracted as the first and last values in the vector $\boldsymbol{P}$,

$$\boldsymbol{y} = [P_1, P_j]^T = \boldsymbol{g}(\boldsymbol{x}). \tag{51}$$

4.2. Temporal Discretisation

The model in (50) is discretised in time by making use of the fourth order explicit Runge-Kutta method with a zero-order hold on the inputs and parameters between sampling intervals. The Runge-Kutta time step size s is a constant enforced by the CFL condition which can be defined for the one-dimensional case as,

$$s \leq \frac{c \, z_{\min}}{v_p^{in}}, \tag{52}$$

where the Courant number c has a value of 1 in the strict sense, but is often chosen to be smaller in practice for improved numeric stability. $z_{\min}$ is the smallest spatially discretised element length $z_n - z_{n-1}$, and v_p^{in} is the pipe inlet linear gas velocity. The CFL condition, in the simplest sense, ensures that the fluid in the pipe does not travel over multiple discretised adjacent space-time grid segments per iteration. The step size s is not varied during the time propagation in this study but chosen to be constant subject to (52). The Courant number c is conservatively chosen to be 0.8.

4.3. SEM Model Verification in Simulation

The verification of models is useful to provide insights into possible approximation errors and neglected dynamics [42]. The choice of pipe segments and polynomial order in the SEM will be verified in a simulation following a procedure recommended by [40]. The choice of pipe segments and polynomial

Table 2: SEM model verification parameters.

Parameter	Value	Units
Initial Inlet Pressure (P_z)	3×10^6	Pa
Initial Outlet Pressure (P_L)	$P_z - \frac{fZR\,TQ\|Q\|L}{2DA^2M_wP_z}$	Pa
Initial Mass Flow (Q)	5	kg/s
Friction (f)	0.4	-
Compressibility (Z)	0.95	-
Gas Constant (R)	8314.47	J/kmolK
Temperature (T)	300	K
Molecular Weight (M_w)	17.2	kg/kmol
Pipe length (L)	5000	m
Pipe Diameter (D)	0.38	m

order is chosen at the values of $n = 1$ and $N = 2$, and iteratively increased until the model output error between iterations becomes sufficiently small. The non-linear model is initialised at the conditions shown in Table 2 and provided with a sequence of inputs to Q_z and Q_L. P_L is initialised from P_z using a simplification of (1b) [1].

It is typically required in practice to increase spatial discretisation for a pipe length longer than 5000m [15]. Therefore, a pipe length of 5000m was chosen for then SEM model verification. The rest of the parameters are chosen to reflect a typical header used for the model validation in Section 5. The states are initialised by interpolating between the boundary conditions. The simulation is propagated using the fourth order Runge-Kutta explicit time discretization scheme. The model parameters f, Z, T, and M_w are assumed constant for the SEM model verification. These assumptions can be made without significant loss in model accuracy (see e.g. [7]) depending on process operating region variability [17].
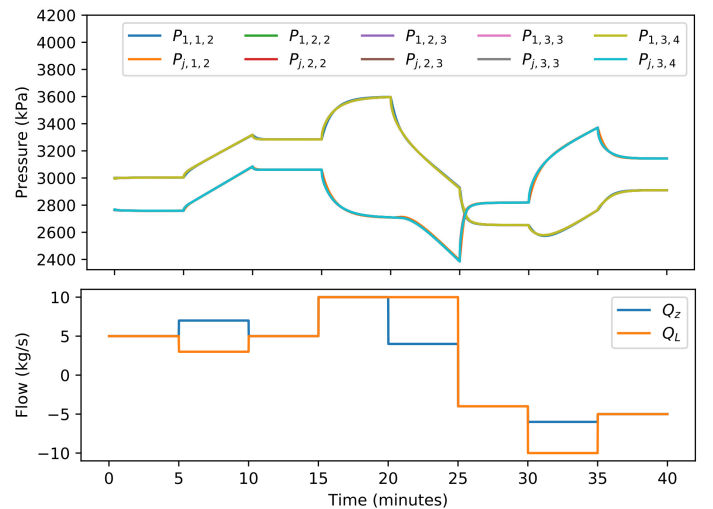

Figure 1: Dynamic responses of the pressure outputs $P_{1,n,N}$ and $P_{j,n,N}$ given flow inputs to Q_z and Q_L for different choices of n and N.

7

The flow input changes Q_z and Q_L, and pressure output responses $P_{1,n,N}$ and $P_{j,n,N}$ for the choice of n and N are shown in Fig. 1. The following qualitative conclusions can be made. A difference in the mass balance leads to a constant change in pressure. The pipe pressure loss is determined by the flow rate magnitude. This tends to zero at low flow rates and increases at higher flow rates. Mass balance off-set, when Q_z and Q_L are not the same, has an integrating pressure response, and flow rate changes have self-regulatory pressure and flow responses. The model accommodates bi-directional flow which inverts the pressure profile. The model outputs are very similar visually, therefore Table 3 has been provided to show quantitative information.

Table 3: Model verification results.

n	N	States	Δ MOE (Pa)	Δ States	(52) (s)
1	2	6	-	-	494
2	2	10	851	4	247
2	3	14	33	4	137
3	3	20	18	6	91
3	4	26	15	6	57

Table 3 shows the choice of n and N, the number of resulting states calculated as $2(nN + 1)$, the change in the mean output error (ΔMOE) between iterations, the change in the number of states between iterations, and the CFL restriction (52). An increase in discretisation improves the model accuracy but also increases computational effort by increasing the amount of states, and decreasing the required time step size. $n = 2$, and $N = 3$ is chosen as a good trade-off between the improved accuracy indicated by the small ΔMOE of 18 Pa in the next iteration, and the increase of 4 states in the chosen iteration as opposed to 6 states in the next iteration. The improvement in accuracy relative to the choice of pipe segments and polynomial order is dependent on pipe length.

5. Validation on an Industrial Network

In this section the developed model is validated on an industrial MRG network using all the property calculations described in Section 2, then discretised spatially using the SEM in Section 3, and simulated in time as described in Section 4.

5.1. Methane-Rich Gas Network Description

The MRG network consists of three headers, Header A, B and C, which are shown in Fig.2, Fig.3, and Fig.4 respectively. Flows which can be manipulated are shown by dashed lines, uncontrolled flows are indicated by thin solid lines and the headers are indicated by thick solid lines. The network has four suppliers of MRG and two suppliers of NG which are divided equally between headers A and B. Header A has two consumers and Header B has three consumers. Both Headers A and B may flare gas with the option of flaring gas on the low pressure side before the MRG supply compressors or after the compressors
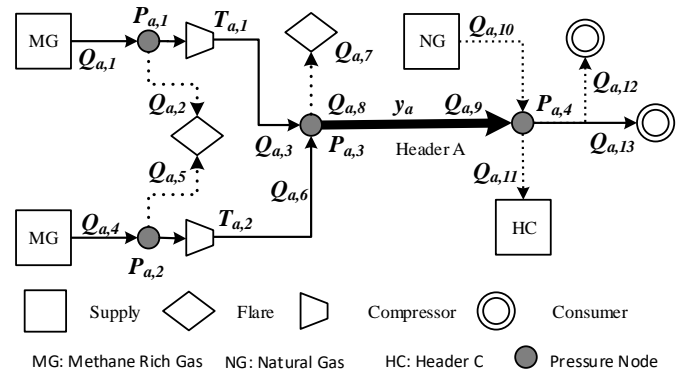

Figure 2: Header A.

on the high pressure side. Header C has 4 consumers and is supplied by both headers A and B but does not have a flare stream. The primary function of the NG is to provide additional gas in low pressure scenarios.

As shown in Fig. 2 and Fig. 3, the header inlet temperatures $T_{a,1}$, $T_{a,2}$, $T_{b,1}$, and $T_{b,2}$ are measured at the MRG compressor discharges. The composition analyses y_a and y_b are measured at header inlets. The unknown parameters are the header inlet and outlet flow rates $Q_{a,3}$, $Q_{a,6}$, $Q_{a,8}$, $Q_{a,9}$, $Q_{b,3}$, $Q_{b,6}$, $Q_{b,8}$, $Q_{b,9}$, $Q_{c,2}$, and $Q_{c,3}$.

5.2. Network Simplification

Simplifying assumptions were made to improve the usability of the MRG network for validation purposes.

- Pressure nodes on opposite sides of short pipe segments with small pressure drops were combined into a single pressure node. This eliminates short pipes with fast dynamics and also erroneous flow direction predictions due to the difference in pressure transmitter readings that fall within the measurement error band.

- Uncontrolled consumer flows originating at the same combined pressure node were grouped into a singled uncontrolled consumer flow which reduces the amount of inputs to the model.
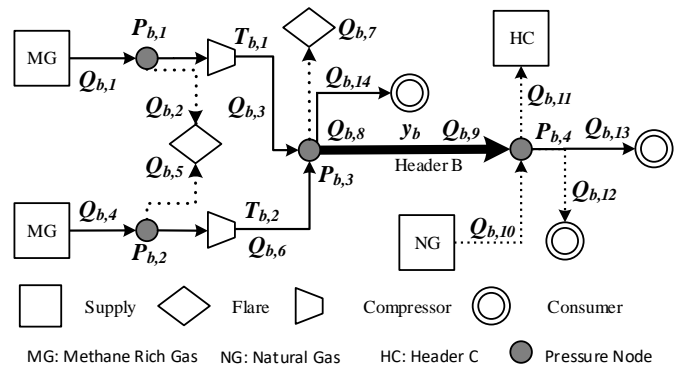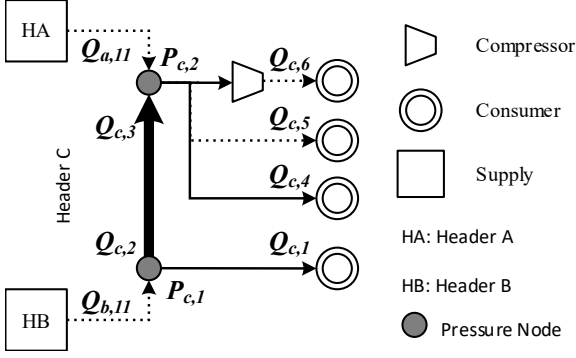

Figure 3: Header B.

Figure 4: Header C.

- The supplier and consumer flow lines are fitted with non-return valves ensuring one-directional flow.

- The natural gas streams enter the network such that they do not enter Header C.

- In this work, the gas properties in (2), (3), (4), (5), (6), (7), and (8) are calculated using the pipe inlet conditions and assumed constant for the pipe length and between sample intervals. This was done because the properties do not change substantially along the pipe length or between sample intervals and reduces the computational effort.

- The control valves and compressors are governed by base-layer controllers and it is assumed that they reach set-point adequately fast and are therefore not directly included in the transient modelling.

- The compressors are not directly included in the model because all the needed header measurements at the suction and discharge ends of the compressors are available. The compressors will need to be considered if economic optimisation is applied to the network because the power consumption will need to be considered as shown by (15). This is because the power consumption is dependent on the suction and discharge header pressures, and flows through the compressors which are used as model inputs.

The flow transmitters are susceptible to measurement, flow-compensation, and instrument calibration errors which cause non-closure in the mass balance of up to 5 percent. To ensure mass balance closure, a pseudo-uncontrolled stream was created which has a calculated value equal to the averaged mass balance closure error with a rolling value greater than the longest time to steady-state of any flow rate. This still allows for dynamic changes to be observed while ensuring steady-state closure for validation purposes. This stream is only used during dynamic validation with real measurements and is not used in a simulation environment. This method is only viable due to the *a priori* information that the header pressures are controlled at set-point, and therefore the mass balance is automatically closed.

5.3. Network Equations

The I flows into and K flows out of each pressure node at steady-state can be related by making use of a mass balance,

$$\sum_{i=1}^{I} Q_i = \sum_{k=1}^{K} Q_k. \tag{53}$$

The pressure continuity over the nodes is given by,

$$P_{J,i}^{in} = P^{node} = P_{1,k}^{out}, \tag{54}$$

for $i = \{0, \ldots, I\}$, and $k = \{0, \ldots, K\}$. $P_{J,i}$ indicates the outlet pressures of the I pipes flowing into the node and $P_{1,j}^{out}$ indicates the inlet pressures of the K pipes flowing out of the node at a pressure of P^{node}. The node temperature T^{node} of a node is a function of the I inlet flow temperatures and their corresponding flow rates,

$$T^{node} = \frac{\sum_{i=1}^{I}(Q_i T_i)}{\sum_{i=1}^{I} Q_i}. \tag{55}$$

To simplify the validation process, (53) is used to calculate the inlet and outlet flows for Header A as,

$$Q_{a,8} = Q_{a,1} - Q_{a,2} + Q_{a,4} - Q_{a,5} - Q_{a,7}, \tag{56a}$$
$$Q_{a,9} = Q_{a,11} + Q_{a,12} + Q_{a,13} - Q_{a,10}. \tag{56b}$$

Similarly to Header A with the exception of an additional flow, the inlet and outlet flows for Header B are calculated as,

$$Q_{b,8} = Q_{b,1} - Q_{b,2} + Q_{b,4} - Q_{b,5} - Q_{b,7} - Q_{b,14}, \tag{57a}$$
$$Q_{b,9} = Q_{b,11} + Q_{b,12} + Q_{b,13} - Q_{b,10}, \tag{57b}$$

and the inlet and outlet flows for Header C are calculated as,

$$Q_{c,2} = Q_{b,11} - Q_{c,1}, \tag{58a}$$
$$Q_{c,3} = Q_{c,4} + Q_{c,5} + Q_{c,6} - Q_{a,11}. \tag{58b}$$

5.4. Parameter Estimation

The unknown parameters used in the validation are the header equivalent pipe lengths and resistance coefficients. The parameters are estimated by making use of an output prediction error method [33], [34], by minimising the objective function $V(\theta)$,

$$\min_{\theta}\left[V(\theta) = \frac{1}{M}\sum_{i=0}^{M}\|y_i - \hat{y}_i\|^2\right], \tag{59}$$

where the fitting parameters are grouped into the vector $\theta = [L_G, K_G]^T$, and $\hat{y}_i$ and y_i are the M predicted outputs and measured outputs at sample time t_i respectively. The estimation was done for a period of 800 minutes on plant data from a different time period than the time period shown in Section 5.5. The fitted constants, and real pipe lengths L_r are shown in Table 4.

It is possible to only use K_G to compensate for component friction, but the combination with L_G provides flexibility in accounting for network volume lost due to the combination of pressure nodes described in Section 5.2.

9

Table 4: Model validation parameters.

Header	L_r (m)	L_G (m)	K_G (m^{-1})
A	800	358	9.3 x 10^5
B	800	384	8.9 x 10^5
C	4000	3468	9.5 x 10^5

5.5. Validation Results

The inputs used for the model validation are shown in Fig. 5. These are the inlet and outlet flow rates of each header, the molecular weights y_a and y_b of Headers A and B respectively, and the header temperatures T_a and T_b, calculated using (55), of Headers A and B respectively. Header C does not have temperature measurements or composition analyses and therefore these parameters are calculated from the inlet flow streams. The molecular weights $M_{w,a}$ and $M_{w,b}$ shown in Fig. 5 are not direct inputs but provide a good indication of the mixed gas composition variability. Table 5 shows the values used to scale, for commercial reasons, the inputs and outputs in Fig. 5 and Fig. 6 respectively to be between 0 and 1 relative to their operating ranges. Therefore, as an hypothetical example, if the operating range of the temperatures is $285K$ to $300K$, $285K$ is scaled to 0 and $300K$ is scaled to 1. Table 5 also gives an indication of the variation in the inputs and validated outputs.

Table 5: Input and output operating ranges.

Parameter	Operating range size	Unit
Pressures	200	kPa
Flows	20	kg/s
Temperatures	15	K
Molecular Weight	1.5	kg/kmol

The pressures were predicted for a period of 800 minutes with the inputs sampled at one minute intervals. Fig. 6 shows the scaled predictions for $P_{a,4}$, $P_{b,4}$ and $P_{c,2}$ using the method described in this paper and that of [1], compared to the scaled actual plant measurements. These outputs are chosen because they are the real measurements from which the industrial MRG headers are currently controlled in closed-loop.

The prediction is done using the real plant measurements of the inputs. An operating period was chosen where Header A experienced set-point changes, Header B remained at a constant set-point while experiencing input disturbances, and Header C's set-point was allowed to drift within limits. This was done to showcase the ability of the model to accurately predict different operating scenarios.

The states are initialised using the real plant measurements by equating the pipe boundary flows and pressures to the starting conditions at $t = 0$, and linearly interpolating between them to initialise the states at the collocation points. The states are not updated with the real measured values throughout the simu-

lation. The SEM tuning parameters used to produce the results are given in Table 6.

Table 6: Simulation tuning parameters per header.

Parameter	Description	Value
n	Number of pipe elements	2
N	Polynomial order	3
r	Ratio between element lengths	v_p^{in}/v_p^{out}

The ratio between the element lengths r was chosen as the ratio between the typical inlet and outlet linear gas flow velocities. However, this is small because the influence of gas compressibility on the linear velocity is not substantial for the length of the pipes in this study. It was included for the sake of completeness.

The Pearson correlation and normalised root mean squared error (NRMSE) of the predicted values compared to the actual pressure measurements are shown in Table 7.

Table 7: Current work compared to measured data.

Figure	Pearson Correlation	NRMSE
6a	0.93	16.3x10^{-5}
6b	0.57	7.3x10^{-5}
6c	0.94	14.5x10^{-5}

The strong positive correlations indicate that the predicted values follow the same linear directional movements when compared to the actual pressure measurements. The low NRMSE values indicate that the model-plant offset is low and that the model gains are accurate. Header B has a lower Pearson correlation and a lower NRMSE relative to the other headers. This is due to $P_{c,2}$ not changing substantially during the simulation. The Pearson correlation and NRMSE of the predicted values compared to [1] are shown in Table 8.

Table 8: Current work compared to [1].

Figure	Pearson Correlation	NRMSE
6a	0.99	3.3x10^{-5}
6b	0.89	5.4x10^{-5}
6c	0.99	3.4x10^{-5}

As seen from Fig. 6 and Table 8, the predictions of the current work compared to [1] are very similar. This shows that the same accuracy is obtained while addressing the shortcomings of [1], which is implicitly adhering to the CFL condition for stability. Additionally, the current work allows for bi-directional flow, and generates pipe pressure and flow profiles. The similarity in results supports the validity of the current work because
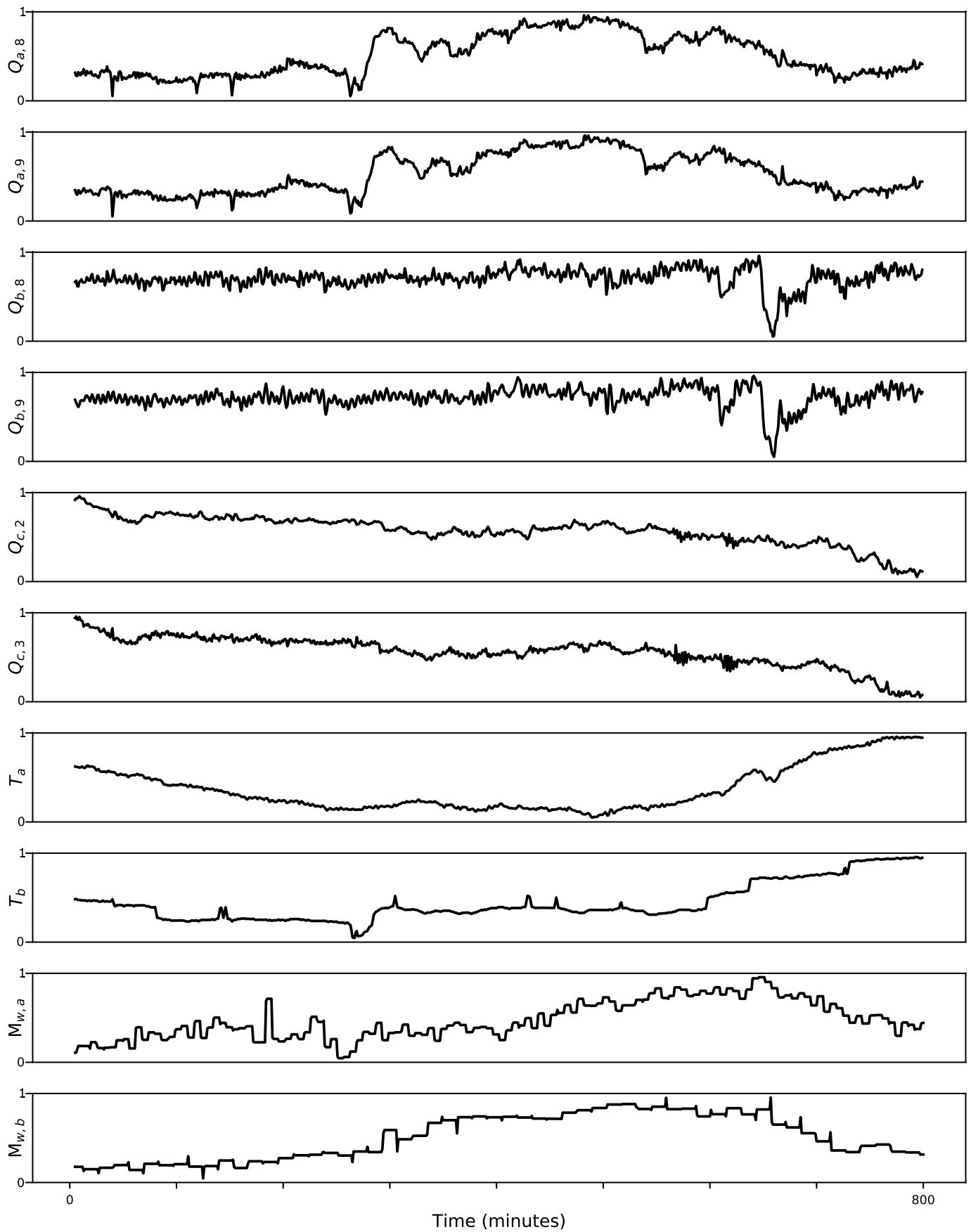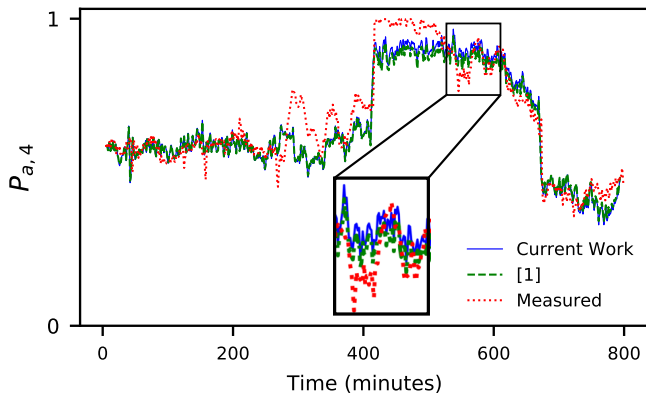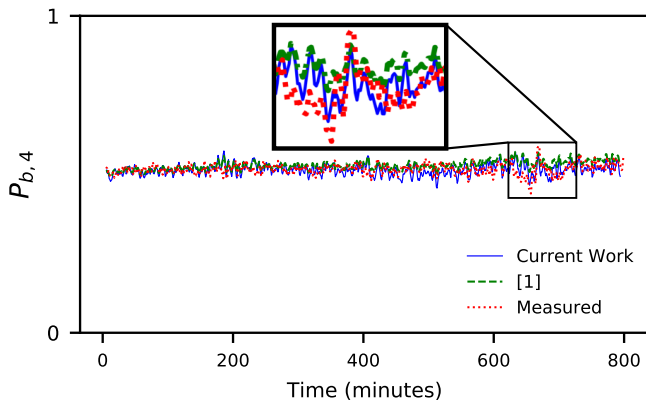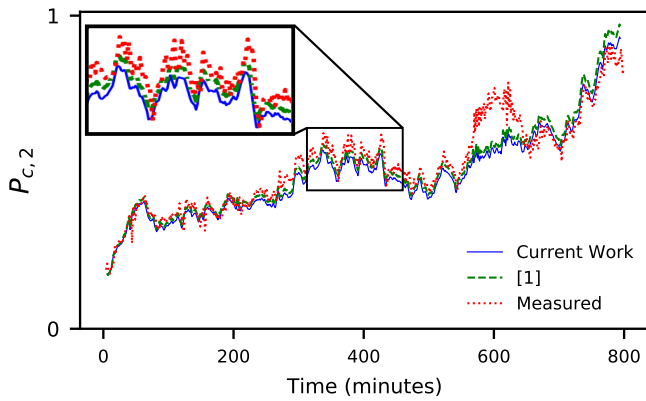
Figure 5: Scaled inputs into the MRG network.

11

(a) Header A

(b) Header B

(c) Header C

Figure 6: Scaled header predictions using the method described in this work compared to the method in [1] and measured plant data.

the model of [1] and the one developed here behave similarly given the same inputs although they were developed differently.

The model-plant mismatch [43], [44] present in Fig. 6 can be attributed to the simplifying model assumptions made earlier and unknown plant disturbances. The error is acceptable as measurement feedback will be able to correct for the error in control applications. The validated model is shown to be able to predict the header pressures accurately.

6. Conclusion

A non-linear model for control applications was developed for an MRG network and validated using real plant measurements. The developed MRG network model uses first principles and empirical models found in literature to model the main components which are combined into a single state-space model. Modelling assumptions made are given to enable modification of the model to fit individual applications. The model accounts for changes in pressure, temperature and composition, as well as changes in consumer and supplier flow rates. Assumptions about the physical layout of the network are used to simplify the model. The SEM was used to spatially discretise the pipelines and develop a system of partial differential equations. The model was developed for an MRG network but, due to the similarity in composition, can also be applied to NG networks. The non-linear model provides accurate predictions of the pressure dynamics over time which can be used to predict the buffering capacity available to reduce flaring and achieve stability in consumer flows.

Future work involves designing and building a multi-variable controller to exploit the buffering capacity of the headers. It was found that parameter estimates are sensitive to initial conditions that can lead to numeric instability if the initial guess is not sufficiently close to a feasible value. A multiple shooting technique [33], [34], as opposed to a single shooting technique used in this article, can be applied to mitigate the sensitivity to initial values in the parameter estimation. The gas temperature as well as the gas properties calculated in Section 2.2, Section 2.3, and Section 2.4 are assumed constant for the entire pipe lengths in the current work. The methodology used in the current work may be expanded to include the energy governing equation for non-insulated pipes, and also to calculate the gas properties at the collocation points for improved accuracy. This will also increase the computational effort and complexity which can be investigated further against the trade-off with accuracy. The model states, that consist of the flows and pressures at the collocation points, provide information regarding the pipe profiles. Applications may exist where the pipe profile information can be made available through suitably designed state estimators.

References

[1] A. J. Wiid, J. D. le Roux, I. K. Craig, Non-linear modelling and validation of an industrial methane rich gas network for control applications, 18th European Control Conference, ECC 2019 8795824 (2019) 3126–3131. doi:10.23919/ECC.2019.8795824.

[2] A. De Klerk, Fischer-Tropsch Refining, John Wiley and Sons, 2012.

[3] C. Muller, I. Craig, N. Ricker, Modelling, validation, and control of an industrial fuel gas blending system, Journal of Process Control 21 (6) (2011) 852–860.

[4] N. Ricker, C. Muller, I. Craig, Fuel-gas blending benchmark for economic performance evaluation of advanced control and state estimation, Journal of Process Control 22 (6) (2012) 968–974.

[5] A. Gopalakrishnan, L. T. Biegler, Economic nonlinear model predictive control for periodic optimal operation of gas pipeline networks, Computers and Chemical Engineering 52 (2013) 90–99.

[6] H. A. Behrooz, R. B. Boozarjomehry, Modeling and state estimation for gas transmission networks, Journal of Natural Gas Science and Engineering 22 (2015) 551–570.

[7] R. Madoliat, E. Khanmirza, H. R. Moetamedzadeh, Transient simulation of gas pipeline networks using intelligent methods, Journal of Natural Gas Science and Engineering 29 (2016) 517–529.

[8] J.-F. Mennemann, L. Marko, J. Schmidt, W. Kemmetmüller, A. Kugi, The spectral element method as an efficient tool for transient simulations of hydraulic systems, Applied Mathematical Modelling 54 (2018) 627–647. doi:10.1016/j.apm.2017.10.010.

[9] J. Strikwerda, Finite difference schemes and partial differential equations, 2nd Edition, SIAM, Philadelphia, USA, 2004.

[10] R. J. LeVeque, Finite volume methods for hyperbolic problems, Cambridge tests in applied mathematics, Cambridge University Press, Cambridge, USA, 2002.

[11] C. Canuto, M. Y. Hussaini, A. Quarteroni, T. A. Zang, Spectral methods: fundamentals in single domains, Scientific Computation, Springer, Berlin, Germany, 2006.

[12] C. Pozrikidis, Finite and spectral element methods using Matlab, 2nd Edition, CRC Press, 2014.

[13] A. Patera, A spectral element method for fluid dynamics - laminar flow in a channel expansion, Journal of Computational Physics 54 (1984) 468–488.

[14] M. Mikolajková, H. Saxén, F. Pettersson, Linearization of an MINLP model and its application to gas distribution optimization, Energy 146 (2018) 156–168.

[15] S. Grundel, N. Hornung, B. Klaassen, P. Benner, T. Clees, Computing surrogates for gas network simulation using model order reduction, in: Surrogate-Based Modeling and Optimization, Springer, 2013, pp. 189–212.

[16] S. Ke, H. Ti, Transient analysis of isothermal gas flow in pipeline network, Chemical Engineering Journal 76 (2) (2000) 169–177.

[17] J. Brouwer, I. Gasser, M. Herty, Gas pipeline models revisited: model hierarchies, nonisothermal models, and simulations of networks, Multiscale Modeling & Simulation 9 (2) (2011) 601–623.

[18] K. Wen, Z. Xia, W. Yu, J. Gong, A new lumped parameter model for natural gas pipelines in state space, Energies 11 (8) (2018) 1971.

[19] B. T. Baumrucker, L. T. Biegler, MPEC strategies for cost optimization of pipeline operations, Computers and Chemical Engineering 34 (2010) 900–913.

[20] Y. Zhou, C. Gu, H. Wu, Y. Song, An equivalent model for gas networks for dynamic analysis of gas-electricity systems, IEEE Transactions on Power Systems 32 (32) (2017) 4255–4264.

[21] A. Herrán-González, J. De La Cruz, B. De Andrés-Toro, J. Risco-Martín, Modeling and simulation of a gas distribution pipeline network, Applied Mathematical Modelling 33 (3) (2009) 1584–1600.

[22] C. A. Dorao, M. Fernandino, Simulation of transients in natural gas pipelines, Journal of Natural Gas Science and Engineering 3 (2011) 349–355.

[23] M. Behbahani-Nejad, A. Bermúdez, M. Shabani, Finite element solution of a new formulation for gas flow in a pipe with source terms, Journal of Natural Gas Science and Engineering 61 (2019) 237–250.

[24] A. Bermúdez, M. Shabani, Finite element solution of isothermal gas flow in a network, Journal of Computational Physics 3 (2019) 349–355.

[25] G. Guandalini, P. Colbertaldo, S. Campanari, Dynamic modeling of natural gas quality within transport pipelines in presence of hydrogen injections, Applied Energy 185 (2017) 1712–1723.

[26] M. Chaczykowski, P. Zarodkiewicz, Simulation of natural gas quality distribution for pipeline systems, Energy 134 (2017) 681–698.

[27] K. Liu, L. T. Biegler, B. Zhang, Q. Chen, Dynamic optimization of natural gas pipeline networks with demand and composition uncertainty, Chemi-

cal Engineering Science 215 (2020) 115449.

[28] M. C. Steinbach, On PDE solution in transient optimization of gas networks, Journal of Computational and Applied Mathematics 203 (2) (2007) 345–361.

[29] A. Zlotnik, M. Chertkov, S. Backhaus, Optimal control of transient flow in natural gas networks, 54th IEEE conference on decision and control (2015) 4563–4570.

[30] R. V. Giles, Fluid mechanics and hydraulics, McGraw-Hill, New York, USA, 1977.

[31] D. Kraft, A software package for sequential quadratic programming, Tech. Rep. DFVLR-FB 88-28, DLR German Aerospace Center – Institute for Flight Mechanics, Koln, Germany (1988).

[32] A. K. Coker, Ludwig's applied process design for chemical petrochemical plants, Volume 1, 4th Edition, Elsevier, Amsterdam, the Netherlands, 2007.

[33] A. H. Ribeiro, L. A. Aguirre, Shooting methods for parameter estimation of output error models, IFAC-PapersOnLine 50 (1) (2017) 13998–14003.

[34] A. V. Rao, A survey of numerical methods for optimal control, Advances in the Astronautical Sciences 135 (1) (2009) 497–528.

[35] A. L. Kareem, T. M. Iwalewa, M. Al-Marhoun, New explicit correlation for the compressibility factor of natural gas: linearized z-factor isotherms, Journal of Petroleum Exploration and Production Technology 6 (3) (2016) 481–492.

[36] Y. Xiaohong, Z. Shunxi, Z. Weiling, A new model for the accurate calculation of natural gas viscosity, Natural Gas Industry B 4 (2017) 100–105.

[37] P. Linstrom, W. Mallard (Eds.), NIST chemistry webbook, NIST standard reference database number 69, National Institute of Standards and Technology, Gaithersburg MD, 20899.
URL https://doi.org/10.18434/T4D303

[38] S. W. Churchill, Friction factor equation spans all fluid flow regimes, Chemical Engineering 84 (1977) 91–92.

[39] D. W. Green, R. H. Perry, Perry's chemical engineers' handbook, 8th Edition, McGraw-Hill, 2008.

[40] H. Igel, Computers, waves, simulations: a practical introduction to numerical methods using Python, Coursera, April, 2019.

[41] J. P. Berrut, L. N. Trefethen, Barycentric Lagrange interpolation, SIAM Review 46 (2004) 501–517.

[42] W. L. Oberkampf, T. G. Trucano, C. Hirsch, Verification, validation, and predictive capability in computational engineering and physics, Applied Mechanics Reviews 57 (5) (2004) 345–384.

[43] S. Skogestad, I. Postlethwaite, Multivariable feedback control analysis and design, 2nd Edition, Wiley, Chichester, England, 2005.

[44] L. Olivier, I. Craig, Model-plant mismatch detection and model update for a run-of-mine ore milling circuit under model predictive control, Journal of Process Control 23 (1) (2013) 100–107.